Hindawi Publishing Corporation
Shock and Vibration
Volume 2015, Article ID 689373, 16 pages
http://dx.doi.org/10.1155/2015/689373

Research Article

Study on Seismic Performance of a Stiffened Steel Plate Shear Wall with Slits

Jin-yu Lu,[1,2] Lu-nan Yan,[1,2] Yi Tang,[1,2] and Heng-hua Wang[1,2]

[1]*Key Lab of Concrete and Prestressed Concrete Structures of Ministry of Education, Nanjing 210096, China*
[2]*School of Civil Engineering, Southeast University, Nanjing 210096, China*

Correspondence should be addressed to Jin-yu Lu; davidjingyu@gmail.com

Received 8 June 2015; Revised 4 August 2015; Accepted 16 August 2015

Academic Editor: Giorgio Dalpiaz

To determine the force mechanism for the steel plate shear wall with slits, the pushover analysis method was used in this study. An estimated equation for the lateral bearing capacity which considered the effect of edge stiffener was proposed. A simplified elastic-plastic analytical model for the stiffened steel slit wall composed of beam elements was presented, where the effects of edge stiffeners were taken into account. The wall-frame analysis model was established, and the geometric parameters were defined. Pushover analysis of two specimens was carried out, and the analysis was validated by comparing the results from the experiment, the shell element model, and a simplified model. The simplified model provided a good prediction of the lateral stiffness and the strength of the steel slit wall, with less than 10% error compared with the experimental results. The mutual effects of the bearing wall and the frame were also predicted correctly. In the end, the seismic performance evaluation of a steel slit wall-frame structure was presented. The results showed that the steel slit wall could prevent the beams and columns from being damaged by an earthquake and that the steel slit wall was an efficient energy dissipation component.

1. Introduction

Steel plate shear wall and its variations are attractive ways for seismic lateral load resisting components for both new and retrofit construction. These designs include steel walls perforated with circular holes [1, 2], steel walls with stiffened large rectangular openings [3], buckling-restrained steel plate shear walls [4], rhombic low yield strength steel plate [5], steel walls with vertical slits [6], and their modified slit configurations [7–9]. The steel slit wall has many remarkable benefits, such as high ductility, capability of high energy dissipation, potential for architectural flexibility, a simple evaluation and adjustment method for the strength and stiffness [6], and a relatively simple fabrication and construction process. Because of its excellent seismic performance and potential for engineering applications, a series of experiments and analytical investigations of its ductility, energy dissipation capacity, and stability behavior were carried out.

Hitaka and Matsui [6] conducted a series of monotonic and cyclic loading tests on steel slit walls. These investigators studied the force mechanism by varying three main slit parameters: width-to-thickness ratio of the link, link length-to-thickness ratio, and number of rows of links. The results showed that the steel slit wall had high ductility and high capability for energy dissipation because the steel slit wall yields before buckling. Adjusting the slit parameters can cause the steel slit walls to effectively avoid premature buckling. Hitaka et al. [10] carried out another series of tests on steel slit walls. In these tests, the effect of the steel frame was taken into account. The tests revealed that, for the walls of medium stiffness, the lateral stiffness and the ultimate strength of the steel slit walls were similar to the results obtained by Hitaka and Matsui [6], but for the steel slit wall with more stiffness, the lateral stiffness and ultimate strength were much smaller than the results obtained by Hitaka and Matsui [6]. The authors attributed this phenomenon to the deformation of the frame, but more detailed analysis was not reported. An equivalent braced model is also proposed that could be employed in commercially available frame analysis programs. Cortés and Liu [11, 12] used the finite element analysis method to study the force mechanism of steel slit walls and steel slit wall-frame structures and performed

a series of experiments to validate the FEA results. The height-to-width ratio of their specimens was 2. In contrast to the test carried out by Hitaka et al. [10], the beam-column nodes of the frame that Cortés used were hinged. Therefore, the steel slit walls resisted the entire horizontal load.

In China, Zhao et al. [13] performed a cyclic loading test on steel slit walls. In this test, they examined 12 specimens using scale models that were 1/4 of the full-scale model. The results indicated that compared with steel slit walls with one row of links most of steel slit walls with two rows of links have higher ultimate strength and lateral stiffness and a fuller hysteresis curve. Ultimate strength and lateral stiffness decrease with increasing link length. Based on the experimental results conducted by Guo et al. [14], it was found that the steel wall got better energy dissipation ability and ductility when the width-to-thickness ratio of a slit column was less than 15 and the height-to-width ratio was over 3. The seismic behavior of steel slit wall was also analyzed on the different seismic waves by Xu et al. [15]. Furthermore, the seismic performance of steel frame-steel plate shear wall with silts was also conducted by tests and numerical simulations under cyclic horizontal load and constant vertical load, for example, Chen et al. [16] and Lu et al. [9]. The design rules for ensuring that the yielding of steel wall precedes the yielding of frame members as well as the sufficient dissipate energy were investigated. Some analytical models for steel slit walls were also proposed. Zhao et al. [17] proposed a simplified model via nonlinear spring elements to conduct the simulations. Based on the stiffness equivalent principle, Shen [18] and Du [19] proposed concentrically braced and cross-braced simplified analytical models. The finite element analysis method was then used to demonstrate the correctness of their models. On the basis of their results, Jiang et al. [20] proposed another type of simplified analytical model called cross brace with two sticks. The test results and the results of the calculation using simplified models are compared to demonstrate the feasibility of his model.

Previous research results have greatly emphasized the engineering applications of the steel slit wall. To provide design suggestions, many specimens were analyzed using ANSYS. Based on the results, reasonable slit parameters were proposed, and the force mechanism for the steel slit wall was clarified. Nevertheless, most software packages used in design engineering offices do not have the ability to model the steel slit wall directly and can rarely consider the nonlinearity of the material in the shell elements. As a continued development of the above analysis, a simplified analytical model is proposed in this paper. It can be a great help for the modeling and analysis of steel slit walls. As the steel slit wall works conjointly with the outer frame structure, it is very important for the expected model to consider their coupled effects. The model proposed in this paper is called a "wall-frame analysis model" and is established based on the mechanical characteristics of the steel slit wall that is subjected to horizontal loads rather than the equivalent stiffness or the equivalent bearing capacity rules. Based on the simplified model, the nonlinear static and dynamic behavior of the shear wall can be determined expediently. Our simplified model can also exactly represent the mutual effects of the shear wall and the frame.

2. Pushover Analysis of the Steel Slit Wall

2.1. Configuration and Finite Element Model of the Steel Slit Wall. The steel slit wall is made from a steel plate with rows of vertical slits separated by equidistant spaces, which forms a series of flexural links between the slits. Figure 1 shows the configuration of the stiffened steel slit wall and all the geometric parameters that define this wall. h, B, and t are the height, width, and thickness of the wall panels, respectively. l and b denote the height and width of flexural links. The width of slit is d. b_s and t_s represent the width and thickness of stiffener. m is the number of flexural links in each row, and n is number of rows. To enhance the stability of the steel slit wall, welded edge stiffeners are usually used along the vertical side of the shear wall [21]. To maximize the stiffness of the steel slit wall, the slits are usually very small. To minimize stress concentrations, a cutting laser is usually used, and a circular arc is used at each slit end [22]. The experimental and numerical research results show that when the slit configuration is designed properly to avoid premature buckling, high ductility and high energy dissipation capability can be achieved simultaneously. The out-of-plane deformation is so small that the forced state of the steel slit wall is similar to the plane stress condition [6].

The four-node finite strain shell element called "SHELL181" is used in ANSYS software package to simulate the steel slit wall. The constitutive model for steel was chosen as the trilinear model with elastic modulus $E = 2.06 \times 10^5\,\mathrm{N/mm^2}$, tangent modulus after yielding $E_t = 0.01E$, yield strength $\sigma_y = 235\,\mathrm{N/mm^2}$, ultimate strength $\sigma_u = 375\,\mathrm{N/mm^2}$, and Poisson ratio $\mu = 0.3$. The Von Mises yield criterion is used to analyze the behavior of the steel slit wall. As boundary conditions, the bottom of the plate is completely fixed, the out-of-plane motion and rotational degree of freedom of the top of the plate are fixed, and the coupling has in-plane translational degrees of freedom. The first buckling mode is introduced as an initial imperfection, and the amplitude is $h/1000$ [23, 24].

For two different specimens, the test result and the calculation result from the finite element model are compared in Figure 2. Figure 2(a) illustrates a specimen (A102) tested by Hitaka and Matsui [6]. Its height-to-width ratio h/B is close to 1. The envelop curve of another specimen (S4) [25] is now presented in Figure 2(b). The geometrical parameters of specimen are $h = 1010\,\mathrm{mm}$, $t = 8\,\mathrm{mm}$, $h/B = 2$, $b_s = 100\,\mathrm{mm}$, $t_s = 8\,\mathrm{mm}$, $m = 1$, $l = 550\,\mathrm{mm}$, $d = 8\,\mathrm{mm}$, and $b = 69\,\mathrm{mm}$. The test setup shown in Figure 3 was designed to apply shear deformations to the steel plate specimens. The horizontal loads were applied on the specimen by means of a hydraulic jack with a 1,000 kN capacity. The load-displacement curve of the finite element analysis is in good agreement with the experimental data. Therefore, the modeling method in this paper is feasible.

2.2. Parameters for the Steel Slit Wall Specimens. According to the statistical data of the calculation [26], 20 specimens were chosen to study the influence of the slit parameters on the performance of the wall panels. The corresponding geometric

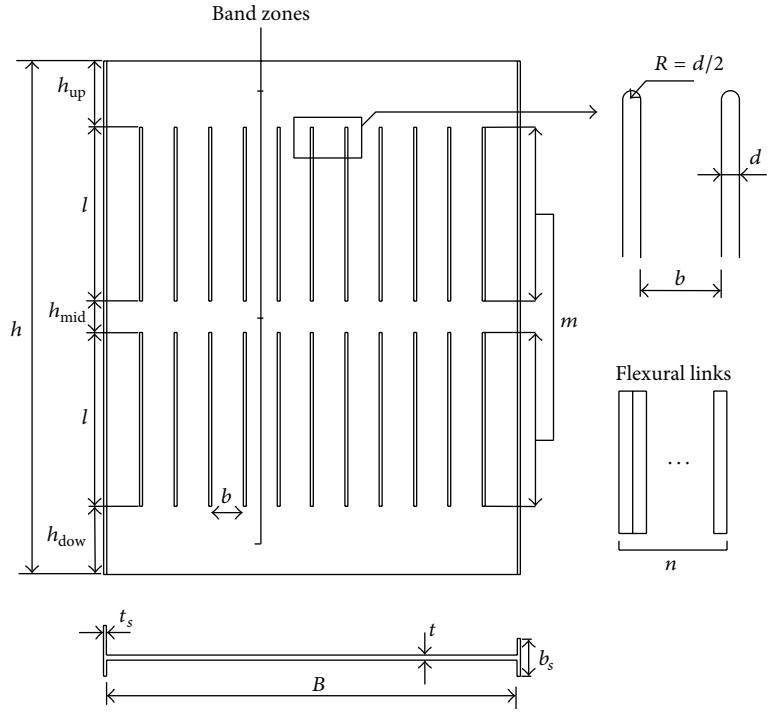

Figure 1: Schematic drawing of steel slit wall.

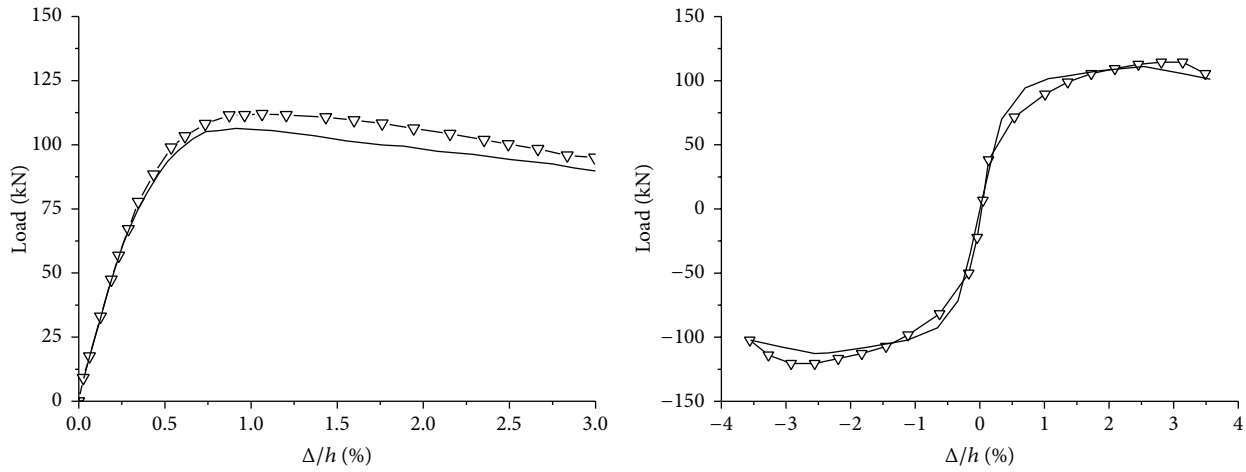

(a) Pushover curve for specimen A102 [6]

(b) Envelope curve for specimen S4 [25]

Figure 2: Verification of the finite element model.

dimensions are summarized in Table 1. The basic geometric dimensions are as follows: $h = 3000$ mm, $d = 15$ mm, $b_s = 220$ mm, $t_s = 15$ mm, and the height-to-width ratio $h/B = 2$.

2.3. Determining the Influence of Different Design Parameters under Pushover Analysis. Figure 4 shows that when the b/h is quite small, the load-displacement curves are very gentle, and the structures show considerable ductility. As the value of b/h increases, the lateral stiffness and ultimate bearing capacity increase significantly, but the load-displacement curves decline suddenly because when the b/h value is quite small, the out-of-plane deformation is quite small, and the failure mode of the wall is in the bending plane of the flexural links that belong to strength failure. The walls yield before buckling. Therefore, the pushover curves do not have a descending branch. As b/h increases, the failure mode becomes the out-of-plane buckling, and the pushover curves decline suddenly in the process of loading.

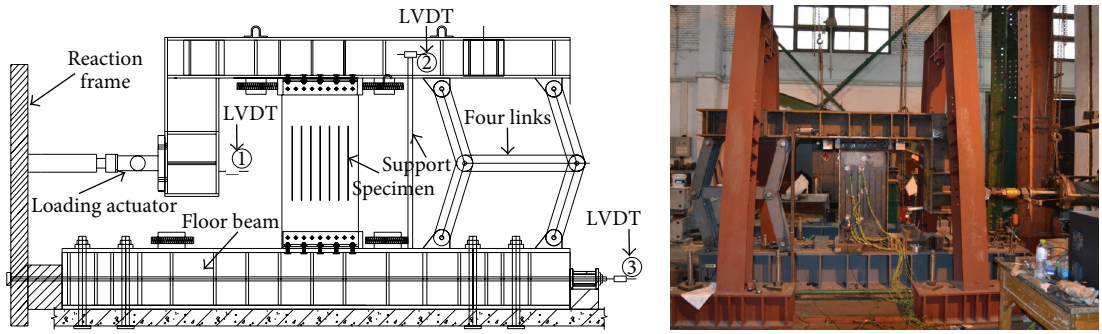

(a) Schematics (b) Photograph

Figure 3: Test setup for specimen S4 [25].

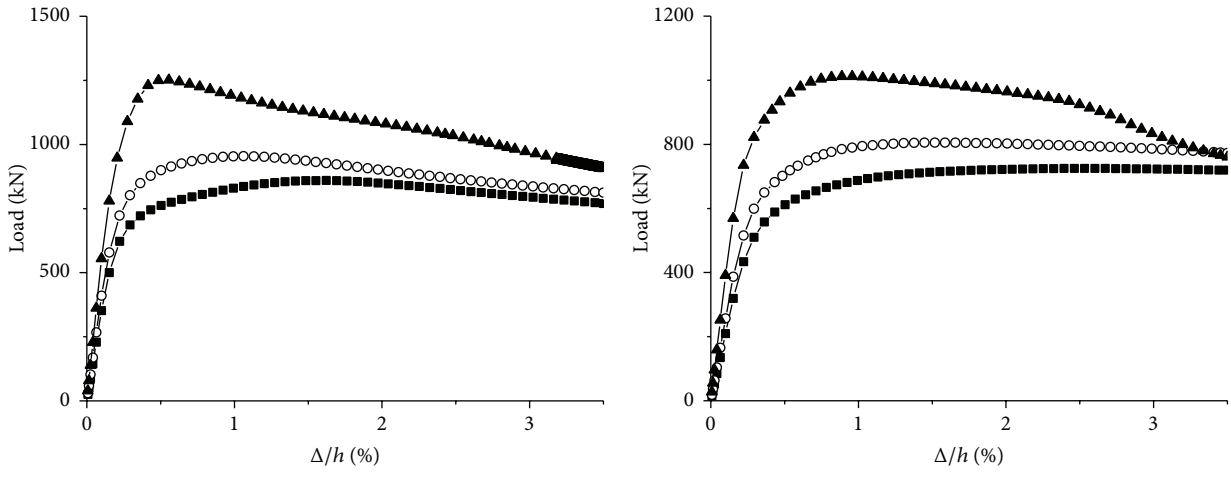

(a) $l/h = 30\%$, $m = 1$ (b) $l/h = 30\%$, $m = 2$

Figure 4: Pushover curves of steel slit walls with different b/h.

Figure 5 shows that the behavior of l/h influences the behavior of the steel slit wall in the same manner as b/h. As l/h decreases, the behavior of the steel slit walls becomes increasingly more like the steel plate without slits. The out-of-plane deformation becomes increasingly larger, and plane buckling of the walls makes the pushover curves drop dramatically during the loading stage.

To express the difference between the pushover curves of the steel slit walls with different h/t values more clearly, the average shearing stress (τ) is used in Figure 6 rather than the load. It shows that h/t has little influence on the lateral stiffness of the steel slit wall. Generally speaking, the descending branch appears more clearly on the pushover curves of walls with larger values of h/t. With the increase in the h/t value, plane buckling becomes progressively easier.

Figure 7 shows that, for the walls that undergo full plastic deformation prior to the out-of-plane buckling, with the increase in m, the lateral stiffness and the ultimate bearing capacity of the steel slit wall increase significantly because the l/h value is decreasing. During the increase in m, the flexural links become shorter and thicker. Under the same load stage, the bending moment at the end of the flexural links becomes smaller, and the ends of the flexural links require a larger lateral load when they begin to yield.

2.4. Mechanical Characteristics of the Steel Slit Wall. The global deformation of the steel slit wall and the free body diagram of a flexural link are shown in Figure 8. The schematic drawing shows that when subjected to horizontal displacement, the steel slit wall undergoes large flexural deformations relative to the shear deformation. The flexural links between the slits behave as beams in a double curvature and work in parallel. The experimental results show that when all flexural links in a given row achieve their plastic moment capacity, the maximum strength of the steel slit wall is reached [6]. To take the effect of the edge stiffener into account, the outmost flexural link is regarded as a T-shaped section (Figure 9). Both the elastic-plastic lateral bearing capacity Q_p

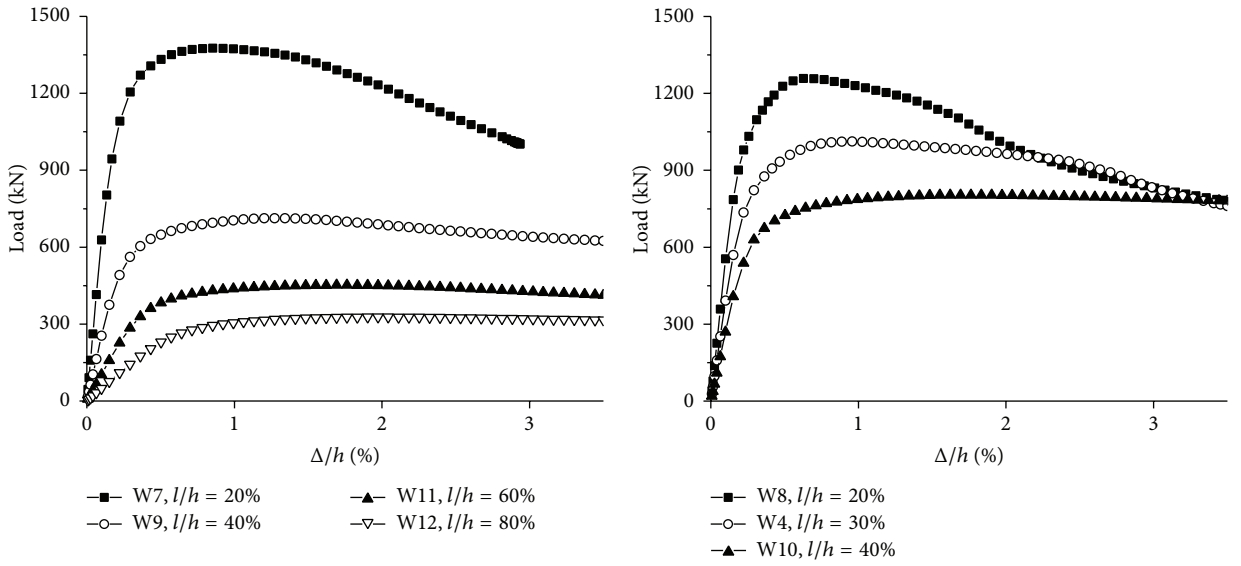

(a) $b/h = 7.067\%$, $m = 1$ (b) $b/h = 7.067\%$, $m = 2$

Figure 5: Pushover curves for steel slit wall with different l/h.

Table 1: Geometric parameters for the steel slit wall.

Specimens number	b/h (%)	l/h (%)	m	h/t
W1	6.104	30	1	200
W2	6.104	30	2	200
W3	7.067	30	1	200
W4	7.067	30	2	200
W5	10.067	30	1	200
W6	10.067	30	2	200
W7	7.067	20	1	200
W8	7.067	20	2	200
W9	7.067	40	1	200
W10	7.067	40	2	200
W11	7.067	60	1	200
W12	7.067	80	1	200
W13	6.104	30	2	150
W14	6.104	30	2	250
W15	6.104	60	1	150
W16	6.104	60	1	200
W17	6.104	60	1	250
W18	7.067	20	3	200
W19	10.067	20	3	200
W20	10.067	60	1	200

and the initial lateral stiffness K_0 of the steel slit wall are illustrated in Figure 10. Q_p is derived and it can be expressed as

$$Q_p = \frac{\sigma_y t}{2l}\left[(n-2)\,b^2 + 4\left(2b_s^2 - b_s t + b^2 - 2e_1 e_2\right)\right]. \quad (1)$$

And (2) is proposed to estimate the initial lateral stiffness of the steel slit wall [6]

$$K_0 = \frac{1}{\kappa\,(h - ml)\,/GBt + (\kappa l/Gbt)\,(m/n) + \left(l^3/Etb^3\right)(m/n)}. \quad (2)$$

The denominator includes three parts to represent the shear deformation of nonslotted regions, the shear deformation of the flexural links between the slits, and the flexural deformation of the flexural links between the slits. Jiang et al. [20] proposed the correction factor: $k(l/b) = (1 + 1.2b/l)^3$, which takes the stress concentration at the end of the flexural links into account. When the width of the slits is small enough and the edge stiffeners are taken into consideration, the equation can be expressed as follows:

$$K_0^* = \frac{1}{\kappa h/GBt + m/\left(2k_{\mathrm{T}} + (n-2)\,k_R\right)}, \quad (3a)$$

$$k_{\mathrm{T}} = \frac{12EI_{\mathrm{T}}}{(l + 1.2b)^3}, \quad (3b)$$

$$k_R = \frac{12EI_R}{(l + 1.2b)^3}, \quad (3c)$$

where k_{T} is the lateral stiffness of the T-shaped section at the two sides of the wall and k_R is the lateral stiffness of the flexural links.

Table 2 illustrates the bearing capacity and the lateral stiffness calculated by formulae and numerical simulations, where e_K represents the errors between results from (2) and simulation and e_K^* represents the errors between results from (3a), (3b), and (3c) and simulation. It shows clear evidence that (3a), (3b), and (3c) provide a good prediction of the lateral stiffness of the steel slit wall, with less than 10% error

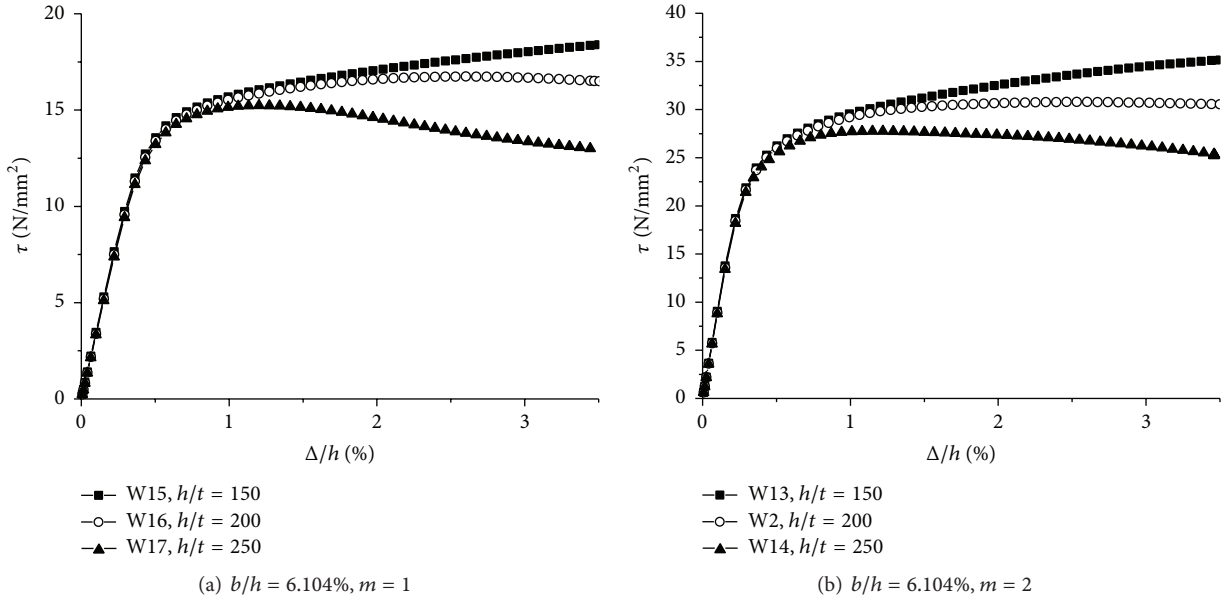

(a) $b/h = 6.104\%$, $m = 1$ (b) $b/h = 6.104\%$, $m = 2$

Figure 6: Pushover curves of steel slit walls with different h/t values.

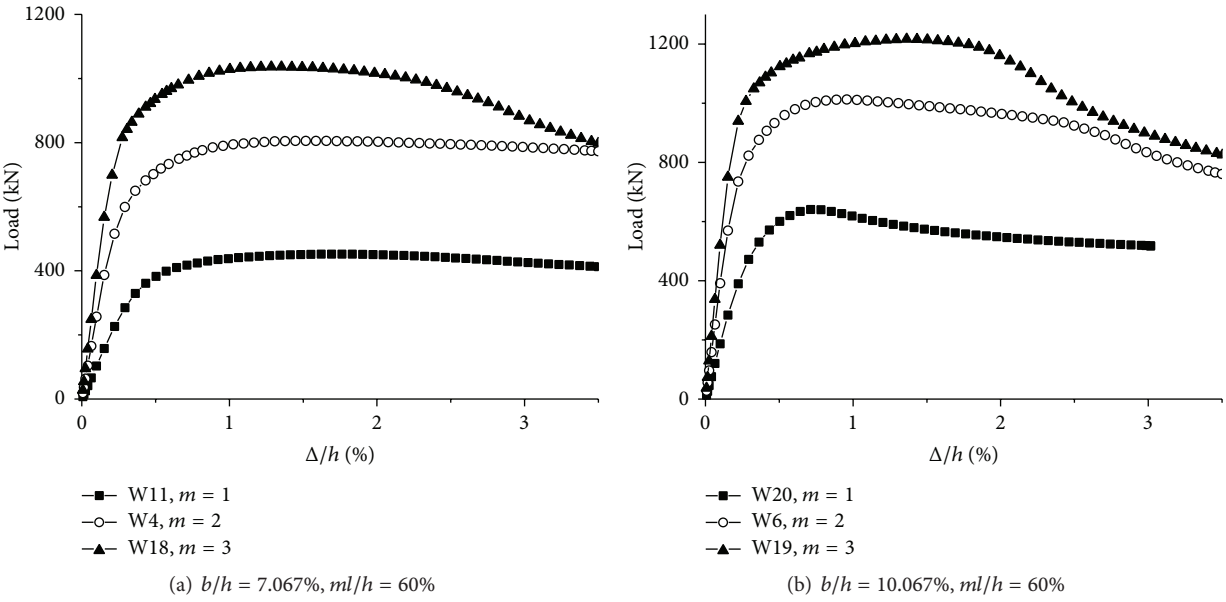

(a) $b/h = 7.067\%$, $ml/h = 60\%$ (b) $b/h = 10.067\%$, $ml/h = 60\%$

Figure 7: Pushover curves of steel slit walls with different values of m.

compared with the experimental results and (1) only applies to estimating strength of the walls with single-layer slits. Some links buckle before yielding during the loading process and the number of yielded flexural links of slit walls with multilayer slits is quite hard to predict. Equation (1) takes only one layer of yielded flexural links into consideration.

Figure 11 shows the structural behavior of the steel slit wall (W20 in Table 1) when the maximum strength is reached. All flexural links develop the plastic moment capacity at their ends, and the yielding of the steel slit wall occurs almost exclusively at these regions (Figure 11(a)). The edge stiffeners develop plastic behavior at the height associated with the end of the flexural links. The external link works like a T-shaped cross section flexural member. From Figure 11(b), we find that the horizontal deformation of the links is almost identical at the same height; that is, the flexural links work in parallel

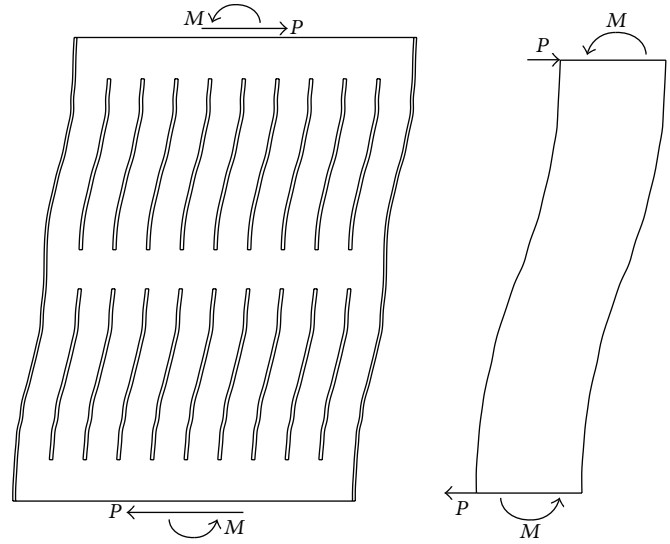

(a) Global deformation

(b) Free body diagram of a flexural link

Figure 8: Lateral deformation of the steel slit wall subjected to horizontal loads.

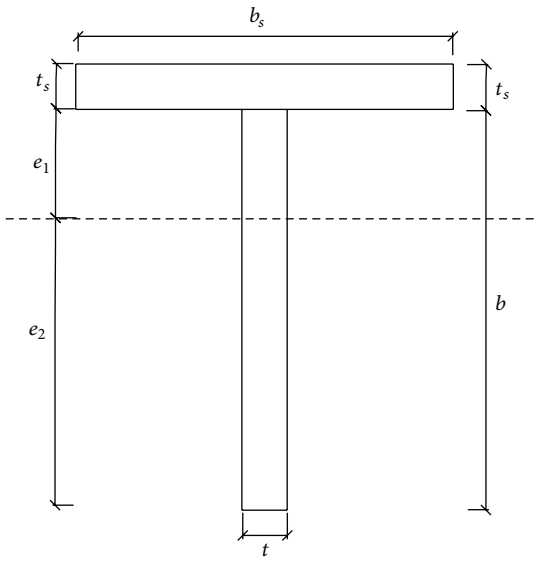

Figure 9: Schematic drawing of edge stiffener.

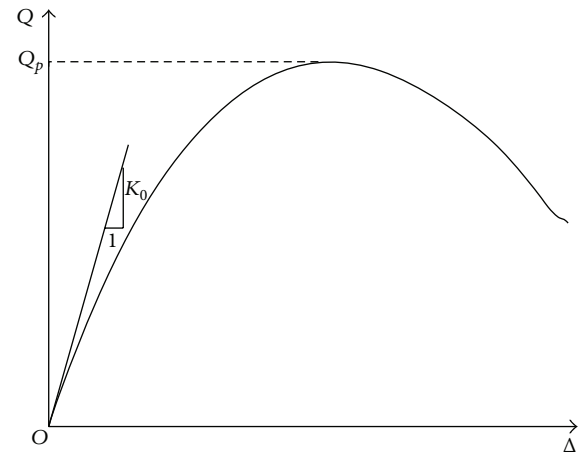

Figure 10: Force-deformation relationships for steel slit walls.

to each other when subjected to horizontal displacement. Figure 11(c) shows that the steel slit wall develops a full plastic moment capacity before buckling. The out-of-plane deformation of the wall is very small, less than half of the thickness of the steel slit wall.

3. Simplified Analytical Model of the Stiffened Steel Slit Wall

3.1. Geometrical Composition of the Simplified Model. Based on the above analysis of the mechanical characteristics of the steel slit wall, the wall-frame analysis model (shown in Figure 12) is presented. The frame element is introduced in the simplified model to simulate the behavior of the steel slit wall rather than the shell element. The geometric parameters that define the simplified model are as follows.

Frame elements labeled as "I," with length l, are used to model the flexural links between the slits. A rectangular cross section $t \times b$ is used in this part. The meanings of the notations (t, b, and l) have been explained in Figure 1. The flexural deformation, the shear deformation, and the axial deformation of the flexural links are all taken into account in the calculation. Frame elements labeled as "II" are used to model the external flexural links of the steel slit wall. A T-shaped cross section is considered, that is, taking the outermost steel plate and the edge stiffener as a compound section. When modeling a steel slit wall, the frame element

Table 2: Initial lateral stiffness and the bearing capacity of the steel slit wall.

Specimens number	Bearing capacity (kN)			Initial lateral stiffness (kN·mm^{-1})				
	Q_p	Q_{FEA}	e_Q (%)	K_0	K_0^*	K_{FEA}	e_K (%)	e_K^* (%)
$m = 1$								
W1	725.37	719.82	0.77	146.27	122.12	119.24	22.68	2.42
W3	860.43	850.75	0.14	179.77	144.82	139.10	29.24	4.12
W5	1279.01	1202.71	6.34	268.22	201.23	188.55	42.25	6.72
W7	1290.64	1241.50	3.96	325.56	253.17	243.26	33.83	4.07
W9	645.32	634.40	1.72	96.05	85.28	84.22	14.05	1.26
W11	444.35	417.63	6.40	32.97	33.39	34.53	−4.51	−3.30
W12	322.66	308.89	4.46	14.47	16.04	15.23	−4.98	5.32
W15	502.76	475.64	5.70	32.95	33.39	36.36	−9.39	−8.18
W16	362.68	351.78	3.10	24.71	25.88	25.69	−3.79	0.77
W17	282.28	274.39	2.87	19.77	20.92	21.04	−6.06	−0.61
W20	639.51	620.64	3.04	63.63	58.19	62.60	1.66	−7.05
$m > 1$								
W2	725.37	639.78	13.38	85.81	69.26	65.03	31.97	6.52
W4	860.43	732.03	17.54	109.82	84.21	85.87	27.89	−1.93
W6	1279.01	941.51	35.85	183.92	124.94	131.19	40.19	−4.77
W8	1290.64	941.09	37.14	242.49	167.65	152.50	59.01	9.94
W10	645.32	517.70	24.65	53.18	54.03	49.85	6.68	8.38
W13	1195.52	864.92	38.22	114.41	90.93	95.26	20.11	−4.54
W14	739.07	491.00	50.52	68.65	57.46	55.55	23.57	3.44
W18	1290.64	941.04	37.15	193.19	131.22	129.39	49.31	1.42
W19	1918.51	1079.53	77.72	282.97	167.55	175.29	61.43	−4.42

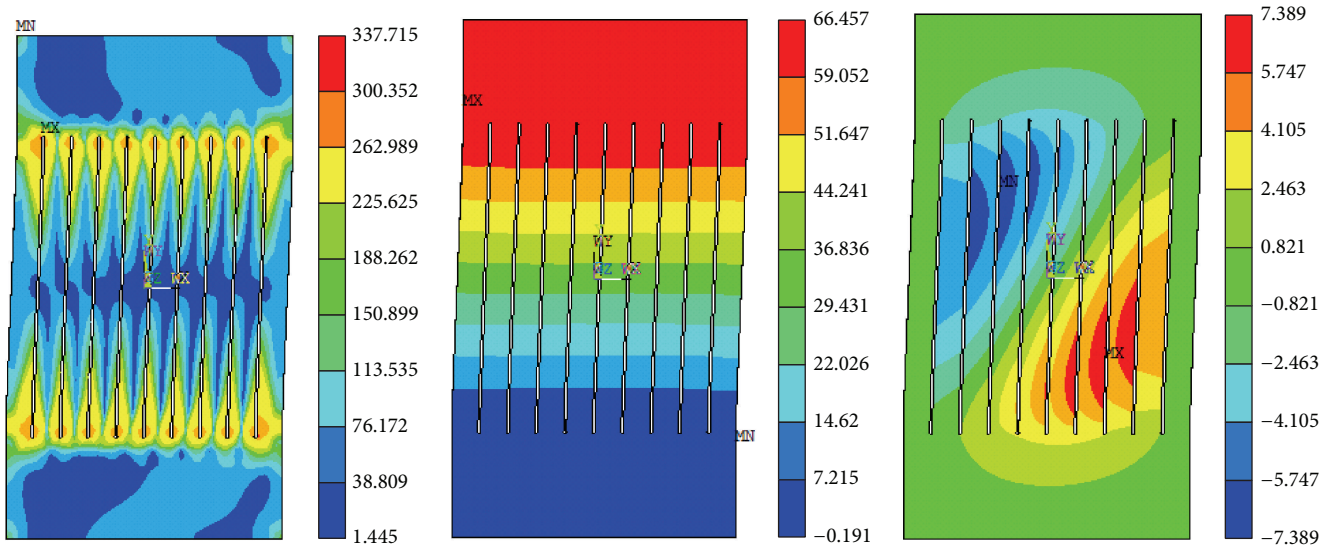

(a) Von Mises stress (N/mm^2) (b) Horizontal displacement (mm) (c) Out-of-plane deformation (mm)

Figure 11: Behavior of the steel slit wall at the ultimate state ($\Delta/h \approx 2.2\%$).

should coincide with the centroid of the T-shaped cross section. Frame elements "III" and "IV" simulate the nonslotted regions above, below, and between the flexural links together, which are referred to as the band zone, as shown in Figure 1. The shear deformation under the horizontal load and the axial deformation under the vertical load are considered in element "III." The height-to-width ratio of the band zone is very small. The flexural deformation under the horizontal load can thus be neglected in the model. The analytical data show that the error resulting from the simplification is very small. The cross section of element "III" can be taken the same as element "I" or "II" connected to it. Element "IV" is used

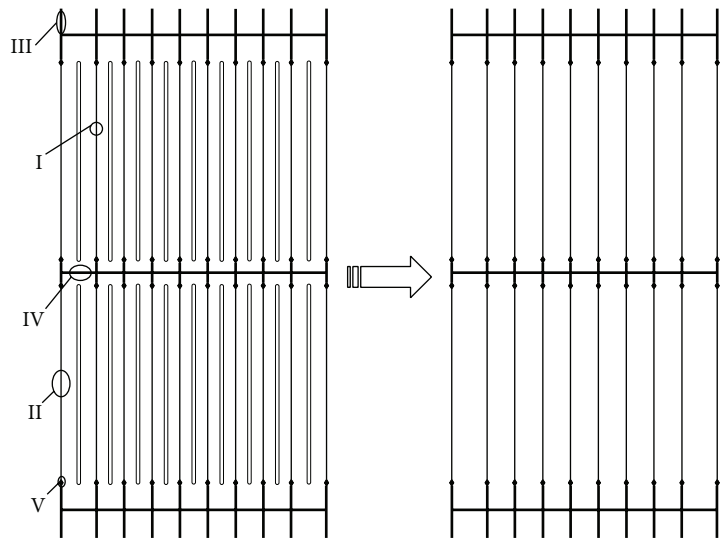

Figure 12: Wall-frame analysis model of the steel slit wall.

to simulate the axial deformation under horizontal load, as well as the shear and flexural deformation under vertical load. According to the location of the elements, $t \times h_{\text{up}}$, $t \times h_{\text{mid}}$, and $t \times h_{\text{dow}}$ are chosen to define the beam sections of element "IV." The flexural deformation of the band zone under the vertical load is taken into account. The black circles "V" located at both ends of the flexural links represent the plastic hinges that account for the material nonlinearity of the steel slit wall. The flexural links can develop full plastic moment capacity at both ends under a large lateral deformation.

3.2. Definition of the Nonlinear Parameters Related to the Plastic Hinge. The definition of the nonlinear parameters related to the plastic hinge is very important because the plastic hinge dictates the global material nonlinear behavior of the steel slit wall. Based on the existing experimental and nonlinear analysis data, a load-deformation relationship curve is defined. Then, the nonlinear parameters related to the moment of the curvature of the plastic hinges are obtained according to the relationship between the global deformation of the steel slit wall and the local deformation of flexural links.

A generalized component of the force-deformation relationship for depicting modeling recommended by ASCE 41 [27] (Figure 13) is employed in the definition of the nonlinear behavior of the steel slit wall. Point B in Figure 13 represents the state that the plastic hinges have developed at the ends of the flexural links. The moment at the ends of the flexural links is given by (4), and the corresponding chord rotation angle is given by (5) as follows:

$$M_E = \sigma_y Z, \tag{4}$$

$$\theta_y = \frac{Q_y}{(hK_0)}, \tag{5}$$

where σ_y is the yield strength of steel, Z is the plastic section modulus of the flexural link, and K_0 is the initial stiffness of the steel slit wall. Typically, when plastic hinges

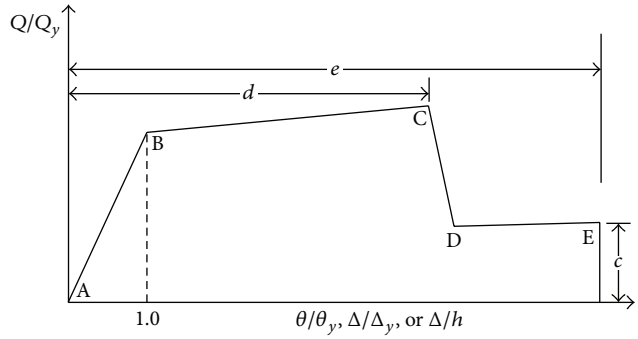

Figure 13: Generalized force-deformation relationships for components.

are assigned to elements "A" and "B," the value of point B can be obtained by a program (e.g., Sap2000 or Midas). However, the steel slit wall produces out-of-plane deformation when it is subjected to a horizontal load. Although the out-of-plane deformation is so little that the buckling of the wall will not occur, there is still an effect on the yield strength [28]. Thus, $0.9Q_y$ is assigned to yield point B [26]. Point C represents the ultimate strength of the component. The abscissa value equals the deformation at which significant degradation of the strength begins (line CD). Based on the experimental and nonlinear analysis database, an ordinate value of $1.0Q_y$ and an abscissa value of 3% are conservatively assigned to the point [27]. Beyond point D, the steel slit wall responds with substantially reduced strength to point E. The residual strength of the point is assumed to be 20% of the yield capacity Q_y. A drift angle of 4% is used to avoid a sharp transition from points C and D, which usually results in computational difficulty and an inability to converge. Point E corresponds to the complete failure of the steel slit wall. The ordinate value of point E is the same as point D, while the abscissa value equals 4.5%. For the deformations greater

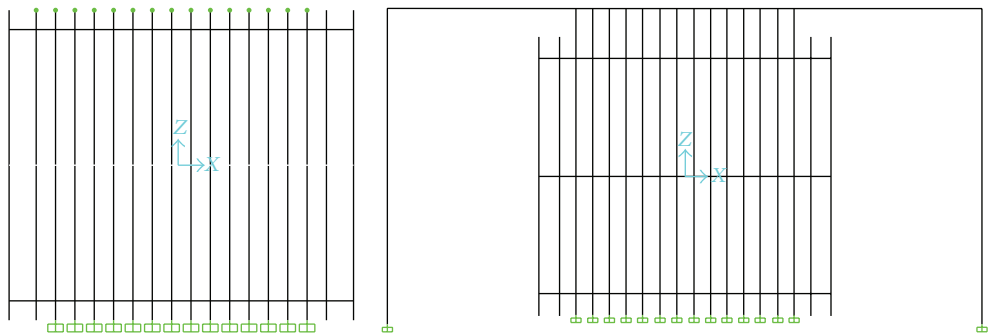

(a) A101 (b) F100W102

Figure 14: Simplified analytical models of two specimens.

Table 3: Geometric parameters for specimens.

Specimens number	b (mm)	l (mm)	m	b_s (mm)	t_s (mm)	Sections of beam and column (mm)
A101	42	512	1	50	4.5	—
F100W102	42	235	2	50	4.5	$100 \times 100 \times 6 \times 8$

than point E, the component strength is essentially zero. After the definition of the nonlinear parameters related to global behavior, conversion of the nonlinear parameters into parameters that prescribe the behavior of the flexural links is necessary. Because the deformation of the band zone is far less than the deformation of the flexural links, all of the deformation is assumed to occur in the slotted region. From the above analysis, it is found that when subjected to horizontal displacement, the flexural links behave as series of beams in double curvature and work in parallel. So the transformation relationship can be expressed as follows:

$$\theta_{\text{link}} = \left(\frac{h}{ml}\right)\theta, \tag{6}$$

where θ is the drift angle of the steel slit wall and θ_{link} is the chord rotational angle of the flexural links.

4. Results and Discussion

4.1. Validation of Simplified Analytical Model. To validate the wall-frame analysis model, the results from two test specimens, A101 [6] and F100W102 [29], are compared to the results from the simplified models. The steel plates for all specimens have dimensions of 800 mm × 800 mm × 4.5 mm, while the boundary conditions are different. A101 is loaded under idealized boundary conditions, while the latter is bounded by a steel moment frame. The validity of the wall-column frame analysis model under two different sets of boundary conditions will be determined in this section. The geometric parameters for the specimens are listed in Table 3.

Figure 14 shows the simplified analytical models of the specimens created in Sap2000. Two accurate models with element SHELL181 are also created in ANSYS. Both material and geometric nonlinearity were considered. Rigid elements were used in the regions on the upper and lower boundaries of the steel slit wall covered by the effective friction surface of the high-strength bolt friction connections.

The load-displacement curves for the tests and different analytical models are shown in Figure 15. The curves from the shell element models and simplified models compare fairly well with the tests. Tables 4 and 5 summarize the initial stiffness and the maximum strength before the 2% drift angle. Subscript "Exp" means experimental results, while subscripts "F," "FEM," and "SM" individually mean results from estimated formulae, finite shell model, and simplified model. The simplified model is observed to provide a good prediction of the stiffness and strength of the steel slit wall, with less than 10% error compared with the experimental results.

Figures 16 and 17 show the moment diagrams of the steel frame from different calculation models under drift angles of 1/500 and 1/100, which correspond to the elastic state and the elastic-plastic state, respectively. The moment diagrams where these diagrams are connected to the steel slit wall are too complicated and relatively small; thus, the moment diagrams are not shown in the figures. For the control sections of the steel frame, the moments obtained from the shell element model are slightly larger than the moments obtained from the wall-frame analytical model by approximately 5%, which means that the simplified analytical model can be used in the designing of a structure containing steel slit walls to account for the additional shear force produced by the steel slit wall.

4.2. Pushover Analysis of Steel Frame-Steel Plate Shear Walls. To illustrate the application of this new simplified analytical model in structural analysis, a 3-story, 4-bay, 3-span steel frame structure was selected as a design example, which is similar to that of references by Cortés and Liu [11, 12]. This steel frame structure is a transverse bearing structure, and its geometric parameters are shown in Figure 18. The uniform dead loads and live loads on the standard floors are individually taken as 4 kN/m^2 and 2 kN/m^2, but 5 kN/m^2 and 2 kN/m^2 on the roofs, respectively. After the preliminary selection, step-by-step trail, and being satisfied with the

Table 4: Comparison of the initial stiffness.

Specimens number	K_{Exp} (kN/mm)	K_F (kN/mm)	K_{FEM} (kN/mm)	K_{SM} (kN/mm)	K_F/K_{Exp}	K_{FEM}/K_{Exp}	K_{SM}/K_{Exp}
A101	8	8.26	7.549	8.1	1.033	0.943	1.013
F100W102	39.2	—	26.3	43	—	1.015	1.096

Table 5: Comparison of the strength.

Specimens number	Q_{Exp} (kN)	Q_F (kN)	Q_{FEM} (kN)	Q_{SM} (kN)	Q_F/Q_{Exp}	Q_{FEM}/Q_{Exp}	Q_{SM}/Q_{Exp}
A101	45	51.038	47.693	42.525	1.134	1.06	0.945
F100W102	236	—	242.2	246.7	—	1.026	1.045

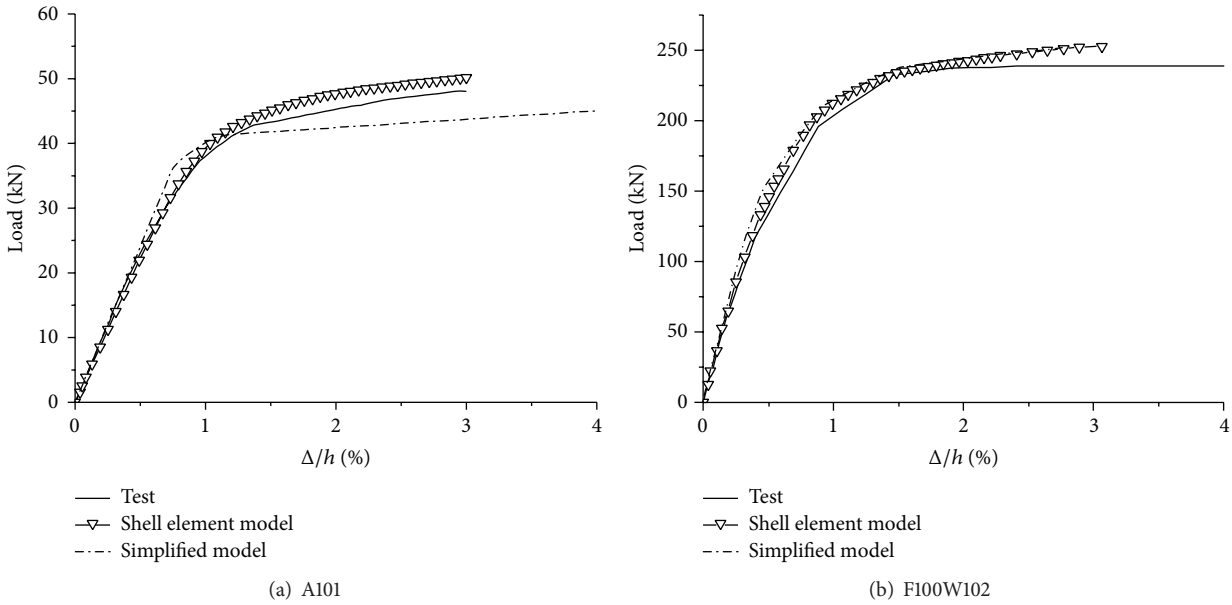

Figure 15: Load-displacement curves from test, shell element model, and simplified model.

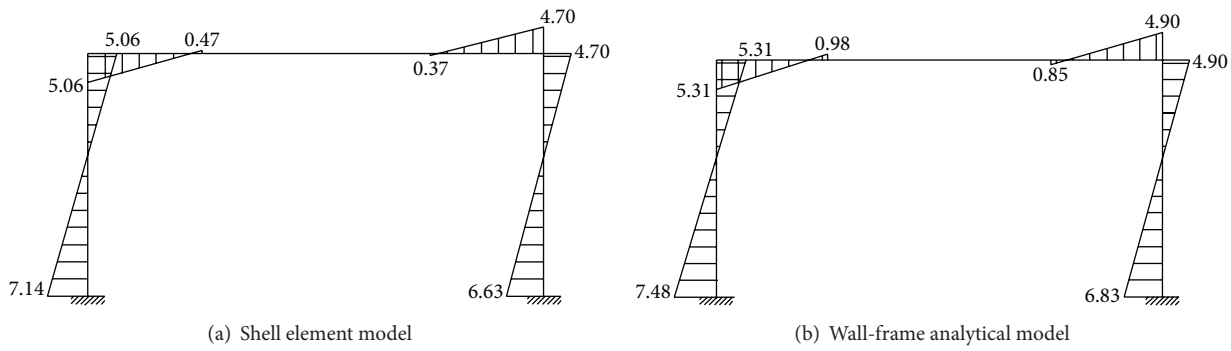

Figure 16: Moment diagrams of the steel frame under the drift angle of 1/500 (kN·m).

corresponding requirements in China design codes, the final sectional dimensions of the I-section beams and columns are determined as follows: transverse beams: 450 mm × 220 mm × 10 mm × 14 mm, longitudinal beams: 400 mm × 200 mm × 8 mm × 12 mm, and columns: 500 mm × 300 mm × 10 mm × 16 mm. For the longitudinal frame, the lateral stiffness of the first story is 37.07 kN/mm and 34.01 kN/mm for the other stories, while, for the transverse frame, the lateral stiffness is 29.66 kN/mm for the first story and 27.21 kN/mm for the other stories.

Based on the principle that the dynamic behavior of the structure in the direction of the two major axes should be similar, we can estimate the lateral stiffness required for the longitudinal frame, such that the lateral stiffness of the first story of the longitudinal frame is 37.07 kN/mm and the lateral stiffness of the other stories is 34.01 kN/mm. To obtain

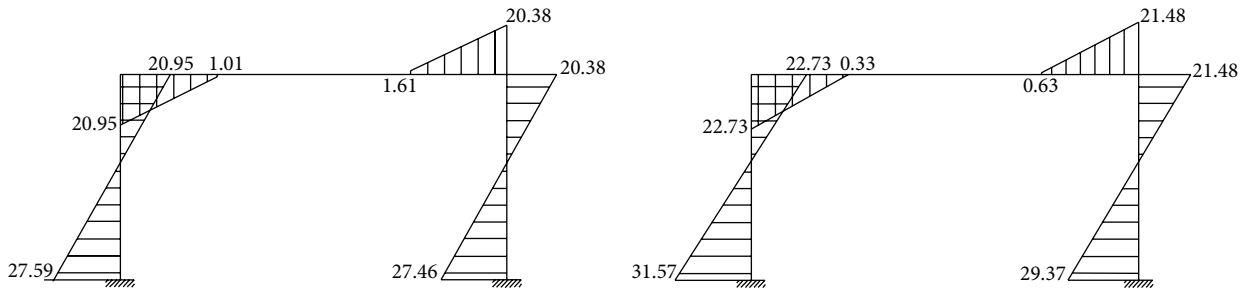

(a) Shell element model (b) Wall-frame analytical model

Figure 17: Moment diagrams of the steel frame under the drift angle of 1/100 (kN·m).

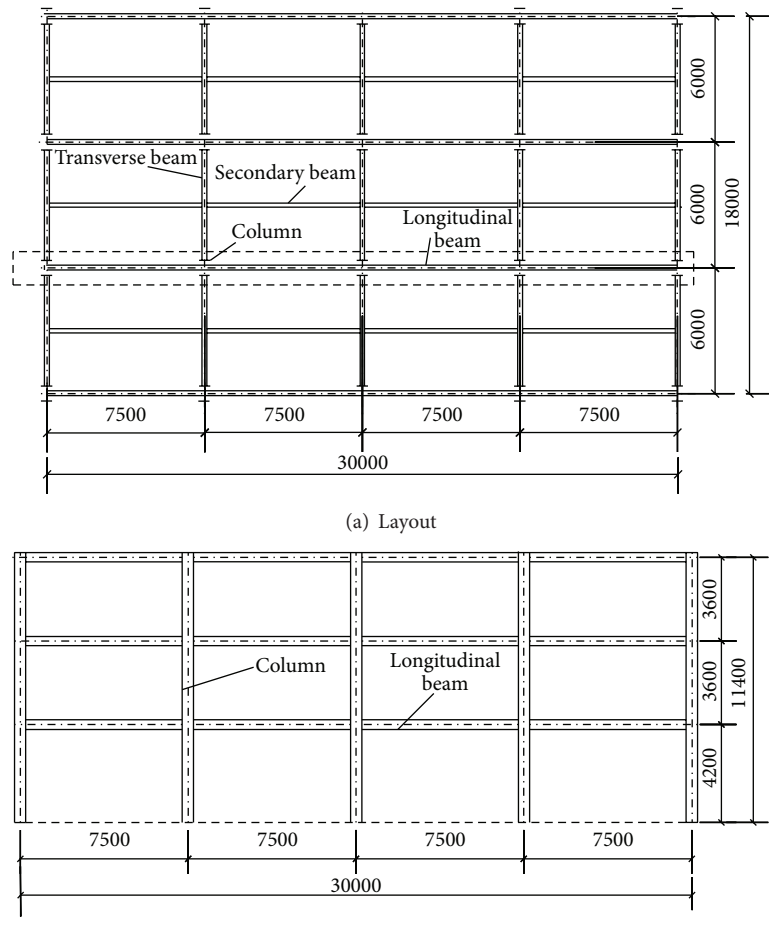

(a) Layout

(b) Elevation

Figure 18: Building scheme (unit: mm).

Table 6: Relevant parameters of the steel slit walls.

Story	m	n	B (mm)	h (mm)	t (mm)	l (mm)	b (mm)	K_0 (kN/mm)
1	2	10	1570	3600	15	1250	143.5	21.79
2~3	1	10	1570	3000	15	1700	143.5	19.37

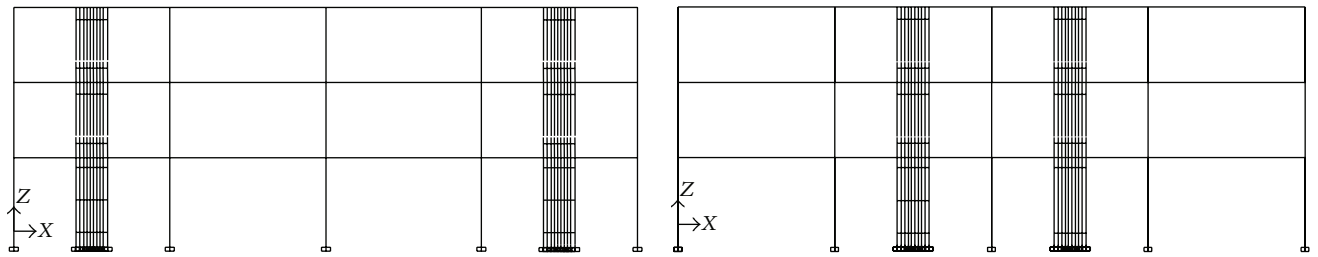

(a) SSFW-1 (b) SSFW-2

Figure 19: Layouts of the steel slit walls.

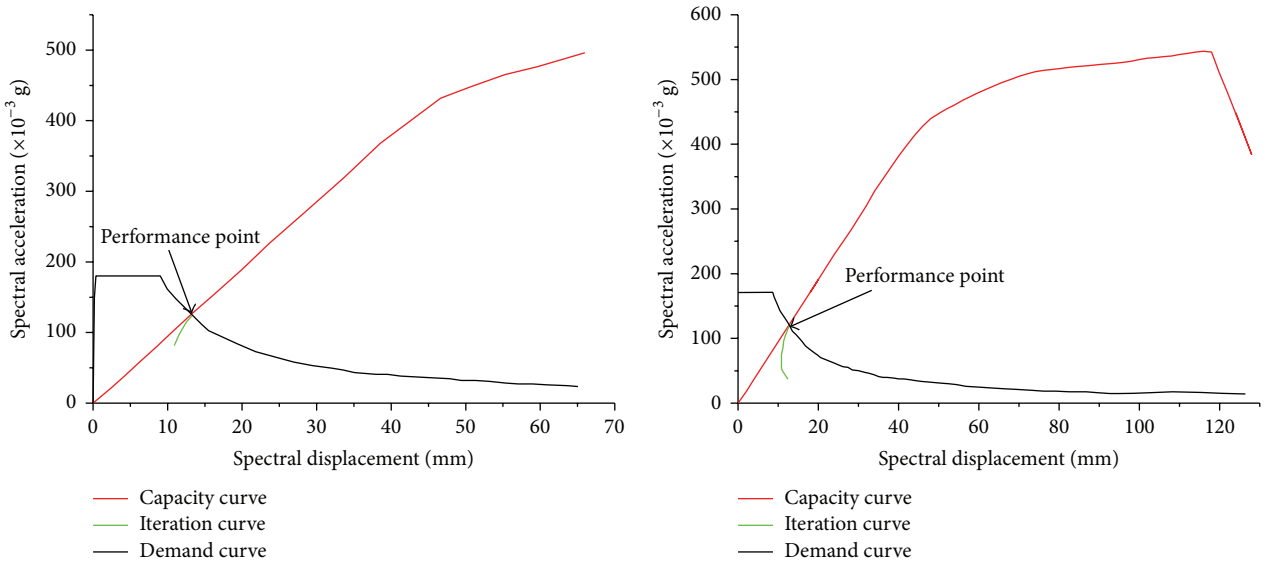

(a) SSFW-1 (b) SSFW-2

Figure 20: Performance point of the different structure under frequent earthquake conditions.

the relevant parameters for the steel slit walls required for each frame, (3a), (3b), and (3c) are used, and the results are summarized in Table 6. Figure 19 shows two frame structures with different layouts of steel slit walls. The pushover analysis method was used to analyze the seismic performance of the two structures under frequent earthquakes and rare earthquakes in the zone of fortification intensity 8 in China [30]. The design basic accelerations of ground motion are 0.2 g and 0.3 g for frequent and rare earthquakes, respectively.

Based on the capacity spectrum method (CSM) [31], the capacity curves of SSFW-1 and SSFW-2 are found to intersect the demand spectrum under frequent earthquake conditions, and their intersections are located on the linear stage of the capacity spectrum (Figure 20). The results show that the SSFW-1 and SSFW-2 remain elastic under frequent earthquake conditions and satisfy the requirements of the code for the seismic design of buildings.

Figure 21 shows that the capacity curves of SSFW-1 and SSFW-2 intersect the demand spectrum under rare earthquake conditions, and their intersections are located on the nonlinear stage of the capacity spectrum. SSFW-1 and SSFW-2 can resist the rare earthquake on the zone of fortification intensity 8 in China, and the structures begin to yield. Figure 22 is the schematic drawing of the plastic hinge distribution on structures under rare earthquake conditions. Plastic hinges appear mainly on the steel slit walls, all columns remain elastic, plastic hinges are formed only on a few beams of SSWF-1, and no plastic hinge is formed on the beams of SSWF-2. This phenomenon indicates that the steel slit walls can be used not only as antilateral force components but also as energy dissipation components to reduce the burden of frames under the earthquake.

The interstory angles of structures under rare earthquake conditions are showed in Figure 23. The interstory drift angles of both SSFW-1 and SSFW-2 under rare earthquake conditions are smaller than 1/50 and satisfy the requirements of the code for the seismic design of buildings. For the performance point, the roof displacements for SSWF-1 and SSWF-2 are 71.61 mm and 71.38 mm, respectively, and the corresponding base reactions are 697.62 kN and 698.42 kN. The roof drift

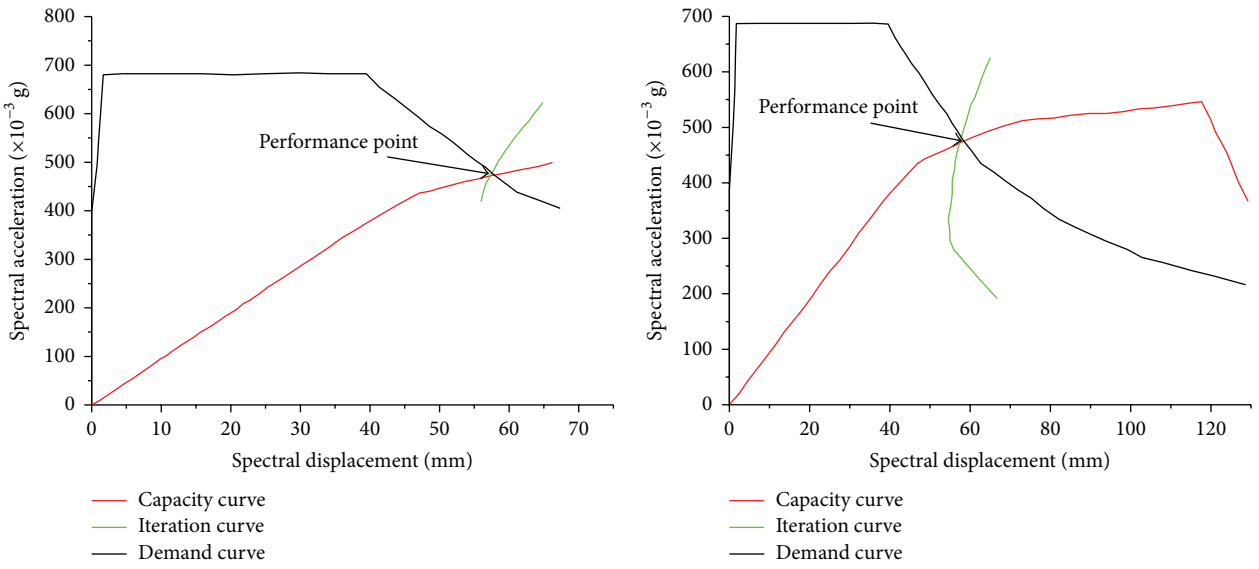

Figure 21: Performance point of the different structures under rare earthquake conditions.

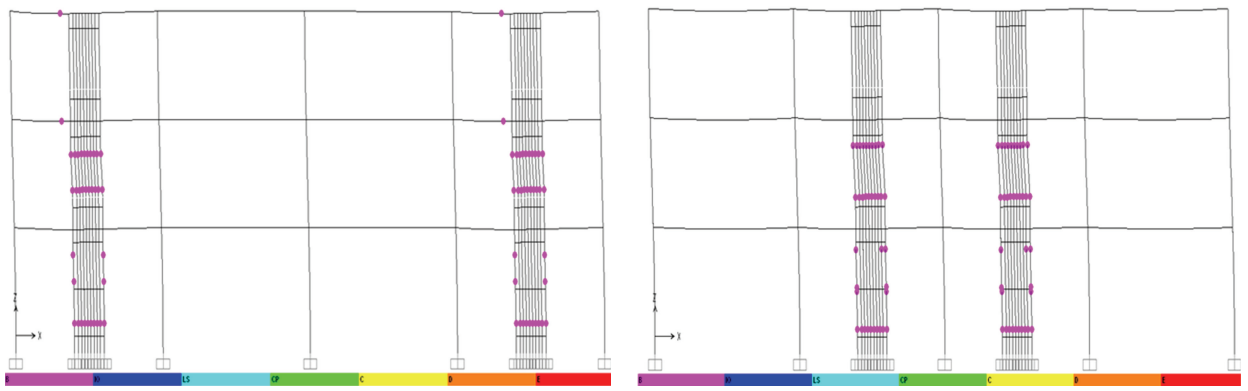

Figure 22: Distribution of plastic hinges.

angles of the two structures are both smaller than 1/50. Overall, the lateral stiffness and the loading capacity of SSFW-1 and SSFW-2 are almost the same. However, from the plastic hinge distribution under rare earthquake conditions, the seismic performance of SSFW-2 is better than that of SSFW-1.

5. Conclusions

Based on the results of the pushover analysis on series of steel slit wall specimens, the effects of the slit parameters, such as b/h, l/h, h/t, and m, on the behavior of the steel slit wall are conducted. An estimated equation for the lateral bearing capacity which considered the effect of edge stiffener is proposed. A reference for designing a steel slit wall is provided. Based on the mechanical characteristics of the steel slit wall, a simplified analytical model named the "wall-frame analytical model" is presented. The simplified model allows for performing nonlinear dynamic and static analysis of structures containing steel slit walls. The parameters related to the configuration and nonlinear behaviors of the simplified model are defined, and the validity of the model is also demonstrated using two specimens. The results show that the load-displacement curves obtained from the simplified model, the shell element model, and experiment agree quite well. The simplified model can correctly predict the mutual effects of the bearing wall and the frame, which must be accounted for in the design. A design example is given, from which the analyzing process of the steel frame-steel slit wall system using proposed simplified model can be learned by the designer.

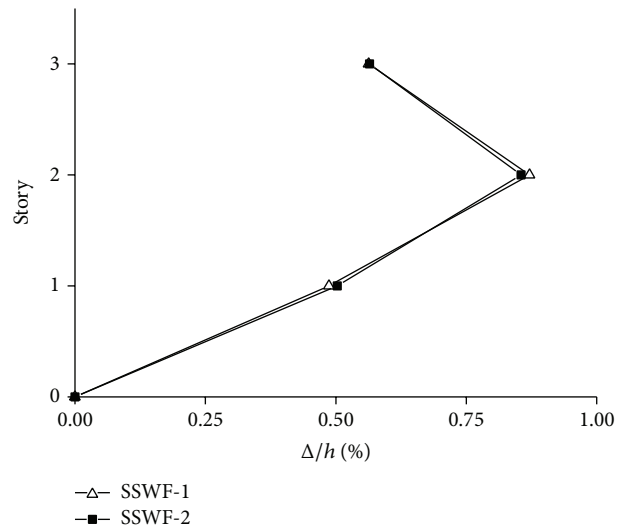

Figure 23: Interstory angles of structures under rare earthquake conditions.

Conflict of Interests

The authors declare that there is no conflict of interests regarding the publication of this paper.

Acknowledgments

The research was supported by the National Natural Science Foundation of China (Grant nos. 51178098, 51208263), the Fundamental Research Funds for the Central Universities and the Excellent Young Teachers Program of Southeast University (no. 2242014R30005), and a project funded by the Priority Academic Program Development of Jiangsu Higher Education Institutions, China. This financial support is gratefully acknowledged.

References

[1] D. Vian, M. Bruneau, K. C. Tsai, and Y.-C. Lin, "Special perforated steel plate shear walls with reduced beam section anchor beams. I: experimental investigation," *Journal of Structural Engineering*, vol. 135, no. 3, pp. 211–220, 2009.

[2] A. K. Bhowmick, "Seismic behavior of steel plate shear walls with centrally placed circular perforations," *Thin-Walled Structures*, vol. 75, pp. 30–42, 2014.

[3] S. A. A. Hosseinzadeh and M. Tehranizadeh, "Introduction of stiffened large rectangular openings in steel plate shear walls," *Journal of Constructional Steel Research*, vol. 77, pp. 180–192, 2012.

[4] M. Amani, B. Rafeei, and M. M. Alinia, "Shear buckling and ultimate capacity of steel plates coupled with cover panels," *Thin-Walled Structures*, vol. 75, pp. 30–42, 2012.

[5] M.-H. Shih, W.-P. Sung, and C.-G. Go, "Investigation of newly developed added damping and stiffness device with low yield strength steel," *Journal of Zhejiang University: Science A*, vol. 5, no. 3, pp. 326–334, 2004.

[6] T. Hitaka and C. Matsui, "Experimental study on steel shear wall with slits," *Journal of Structural Engineering*, vol. 129, no. 5, pp. 586–595, 2003.

[7] A. Jacobsen, T. Hitaka, and M. Nakashima, "Online test of building frame with slit-wall dampers capable of condition assessment," *Journal of Constructional Steel Research*, vol. 66, no. 11, pp. 1320–1329, 2010.

[8] J.-Y. Lu, Y. Tang, G.-P. Shu, and H.-H. Wang, "Hysteretic behavior of steel plate shear wall with slits of unequal length," *Journal of Zhejiang University*, vol. 48, no. 11, pp. 1968–1975, 2014 (Chinese).

[9] J. Y. Lu, Y. Tang, G. P. Shu, H. H. Wang, and N. Li, "Numerical analysis on seismic behavior of frame-novel steel plate shear wall with slits," *China Civil Engineering Journal*, vol. 47, pp. 14–20, 2014 (Chinese).

[10] T. Hitaka, C. Matsui, and J. Sakai, "Cyclic tests on steel and concrete-filled tube frames with slit walls," *Earthquake Engineering and Structural Dynamics*, vol. 36, no. 6, pp. 707–727, 2007.

[11] G. Cortés and J. Liu, "Lateral resistance using steel slit panel frames (SSPFs)," in *Proceedings of the Structures Congress*, pp. 1447–1451, Austin, Tex, USA, April 2009.

[12] G. Cortés and J. Liu, "Experimental evaluation of steel slit panel-frames for seismic resistance," *Journal of Constructional Steel Research*, vol. 67, no. 2, pp. 181–191, 2011.

[13] Z. Z. Zhao, M. Xiao, and J. R. Qian, "Experimental study on seismic behavior of steel plate shear walls with vertical slits," *Building Structure*, vol. 37, no. 12, pp. 105–109, 2007 (Chinese).

[14] L.-H. Guo, X.-B. Ma, and S.-M. Zhang, "Experimental research on steel plate shear wall with slits," *Gongcheng Lixue/Engineering Mechanics*, vol. 29, no. 3, pp. 133–142, 2012 (Chinese).

[15] S. Xu, J. Liu, and T. Peng, "Finite element analysis of seismic behavior of steel plate shear wall with slits," in *Proceedings of the 6th International Conference on Measuring Technology and Mechatronics Automation*, pp. 284–286, IEEE, Zhangjiajie, China, January 2014.

[16] Y. Y. Chen, Y. Ning, and L. Jiang, "Experimental study on seismic behavior of frame-steel plate shear wall with slits," *Journal of Building Structures*, vol. 33, no. 7, pp. 133–172, 2012 (Chinese).

[17] Z. Z. Zhao, M. Xiao, J. Ke et al., "Steel plate shear wall with vertical slips and its trial application in a high-rise steel frame building structure," *Journal of Building Structures*, vol. 31, no. 9, pp. 9–15, 2010 (Chinese).

[18] W. W. Shen, *Elastic simplified model studies of steel plate shear wall with slits [M.S. thesis]*, Xi'an University of Architecture and Technology, Xi'an, China, 2009, (Chinese).

[19] J. H. Du, *The substitution analysis between steel shear wall with slits and concentrically brace [M.S. thesis]*, Zhejiang University of Technology, Hangzhou, China, 2009 (Chinese).

[20] L. Jiang, Y. Y. Chen, and W. D. Wang, "Research on elastic lateral stiffness and simplified model of steel pate shear wall with slits," *Journal of Architecture and Civil Engineering*, vol. 27, no. 3, pp. 115–120, 2010 (Chinese).

[21] J. Y. Lu, S. G. Fan, L. N. Yan, and H. H. Wang, "Simplified elasto-plastic analytical model for stiffened steel plate shear wall with slits," *Journal of Civil, Architectural & Environmental Engineering*, vol. 35, no. 2, pp. 48–53, 2013 (Chinese).

[22] H. Y. Chen, *Experimental studies and theoretical analysis of steel plate shear wall with slits [M.S. thesis]*, Tianjin University, Tianjin, China, 2008 (Chinese).

[23] L. H. Guo, Q. Rong, X. B. Ma, and S. Zhang, "Behavior of steel plate shear wall connected to frame beams only," *International Journal of Steel Structures*, vol. 11, no. 4, pp. 467–479, 2011.

[24] Y. F. Mohtaram, J. T. Kahnamouei, M. Shariati, and B. Behjat, "Experimental and numerical investigation of buckling in rectangular steel plates with groove-shaped cutouts," *Journal of Zhejiang University: Science A*, vol. 13, no. 6, pp. 469–480, 2012.

[25] Y. Tang, *Theory analysis and experimental study on seismic behavior of steel plate shear wall with slits [M.S. thesis]*, Southeast University, Nanjing, China, 2014 (Chinese).

[26] L. N. Yan, *Research on stability and hysteretic behavior of steel plate shear wall with slits [M.S. thesis]*, Southeast University, Nanjing, China, 2011 (Chinese).

[27] American Society of Civil Engineers, *ASCE 41. Seismic Rehabilitation of Existing Buildings*, American Society of Civil Engineers, Reston, Va, USA, 2007.

[28] W. F. Chen and E. M. Liu, *Stability Design of Steel Frames*, CRC Press, Boca Raton, Fla, USA, 1991.

[29] T. Hitaka, C. Matsui, K. Tsudak, and Y. Sadakane, "Elastic-plastic behavior of building steel frame with steel bearing wall with slits," in *Proceedings of the 12th World Conference on Earthquake Engineering (12WCEE '00)*, Auckland, New Zealand, January-February 2000.

[30] National Standard of the People's Republic of China, "Code for seismic design of buildings," Tech. Rep. GB50011-2010, Ministry of Construction of the People's Republic of China, Beijing, China, 2010 (Chinese).

[31] Applied Technology Council, "Improvement of nonlinear static seismic analysis procedures," Report FEMA 440, Federal Emergency Management Agency, Washington, DC, USA, 2005.